

Article

Computer-Aided Environmental Assessment Applied for Estimation of Ecological Impacts Derived from Topological Pathways Based on Lignocellulosic Biomass Transformation

Samir Isaac Meramo-Hurtado ^{1,*} , Plinio Puello ²  and Julio Rodríguez ²

¹ Industrial Engineering Program, Fundación Universitaria Colombo Internacional, Cartagena 130015, Colombia

² Systems Engineering Program, Universidad de Cartagena, Cartagena 1300015, Colombia; ppuellom@unicartagena.edu.co (P.P.); jrodriguezr@unicartagena.edu.co (J.R.)

* Correspondence: smeramoh@unicartagena.edu.co; Tel.: +57-301-6915-157

Received: 22 July 2020; Accepted: 18 September 2020; Published: 21 September 2020



Abstract: The growing awareness to include sustainability goals in the chemical process design has been making palpable since many governments and research institutions have made many efforts precisely to progress new ways to transform available resources into valuable chemicals. In this sense, this work is presenting a computer-aided evaluation based on environmental impact assessment and comparison of technical parameters for estimating the potential effects of two biorefinery designs. The first process involved a multiproduct production of acetone, butanol, and ethanol from cassava waste, while the second biorefinery comprised of succinic acid and bioethanol production from a mixture of cassava waste and banana rachis. These residues are highly available in the North Colombia region due to the agroindustrial activities of that zone. The developed environmental analysis employed the waste reduction algorithm (WAR) for estimating impact generation and output rates considering atmospheric and toxicological categories. Otherwise, process simulation of biorefineries showed production of 546.3 kg/h of acetone, 280.0 kg/h of ethanol, and 1305 kg/h of butanol for topology 1, while topology 2 delivered a synthesis of 13,865.7 kg/h of acetic acid and 2277.9 kg/h of ethanol. Data generated from process simulation allowed performing a technical comparison between evaluated biorefineries, showing a higher performance of evaluated indicators for topology 2. These evaluated variables included resource energy efficiency, and production yield, among others. The environmental analysis provided relevant information, indicating that topology 2 is a better alternative from an ecological viewpoint since this design would emit substances with lower effects than topology 1.

Keywords: computer-aided process engineering; Aspen Plus; environmental analysis; biorefineries; succinic acid

1. Introduction

The cleaner production and resource conservation principles have emerged as obligated aspects that needed to be included in the design of new process technologies. It is worth mentioning that since decades ago, the chemical industry has started changing its traditional conception in order to move into a more sustainable framework, considering the known effects derived from the use of fossil fuels and conventional technologies [1]. The above involved the change in the traditional conceptualization of a chemical process, aiming to progress novel ways that embody environmental impact mitigation, resource conservation, and inclusion of strategies to increase productivity [2]. Since

the first industrial revolution, the activities of many sectors have increased in order to meet higher quality standards [3]. It should be noted that even though society has been capable of achieving very high living standards during the past century, this development has brought consequences over the environment, counting massive amounts of CO₂ and greenhouse gases (GHG) derived from the industrial progress [4]. So, governmental institutions and scientists have identified that the development of new technologies based on sustainable design principles is a must in order to increase the efforts for mitigating the effects of the global economy into the biosphere [5].

The aim of a sustainable chemical process implies the improvement of energy efficiency, seeking the best environmental performance, increase profitability, and using renewable resources [6]. Biorefineries have been established as promising alternatives for sustainably produced biofuels, intermediates, and derivatives, from the use of biomass (renewable resource), which provides advantages over fossil-based processes [7]. In this sense, many contributions have been addressed regarding the design of sustainable biorefineries. Lopez-Linares et al. [8] designed an ethanol production process from hemicellulosic sugars using *Escherichia coli* as a biocatalyzer. Mixed-integer nonlinear programming was implemented to synthesize a profitable biorefinery for producing alcohol from agricultural wastes [9]. Nhien et al. [10] developed a heat integrated and intensified biorefinery design for bioethanol production from lignocellulosic biomass. Multiproduct designs are widespread in biomass transformation processes; for example, a multiproduct biorefinery for the production of bioethanol and lignin was introduced by Davila et al. [11] through a separate saccharification and fermentation pathway.

The recent efforts that have been made for advancing biorefinery design is palpable, but it also is relevant to mention that there remain issues regarding the progress of this type of industry. These limitations involve delays as a result of high scaling up costs, enormous energy demand, and need for specialized equipment, among others that have made that construction of these plants to be currently unpractical and not economical [12]. So, the addition of technical performance parameters and process evaluation techniques is a crucial task in advance of this field [13]. Therefore, environmental analysis arises as a strategic decision-making tool in the process analysis that permits to diagnose and quantify ecological effects derived from the operation of both existing or developing chemical processes [14]. A variety of methods for the quantification of environmental performance are available in the literature; these include the tool for the reduction and assessment of chemical and other impacts (TRACI) [15], the waste reduction algorithm (WAR) [16], or the life cycle assessment (LCA) [17]. Recent contributions have addressed that implementation of an environmental analysis provides useful insights and allows a straightforward comparison between process alternatives. The environmental assessment was implemented for the selection of bio-oil processes from algal and waste biomasses [18]. Alonso-Fariñas et al. [19] implemented environmental analysis for the valorization of mild olive wastes comparing processes based on anaerobic digestion and oil extraction.

As explained, some studies have addressed the use of an environmental analysis for chemical process evaluation; in this sense, this work incorporated the examination of environmental issues through the WAR methodology as a decision-making tool in the evaluation and comparison of promising alternatives of biorefinery design based on the biochemical transformation of lignocellulosic residues. Besides, the proposed procedure included process modeling and simulation of topologies, combined with environmental assessment and technical parameter examination based on the data generated from the studies' processes. It is worth mentioning that the topological pathways examined in this work represent alternatives for waste valorization and solid residue management. The above considering these biorefinery designs are based on the transformation of corn stover and cassava crantz, which are residues highly available in the North Colombia region.

2. Materials and Methods

This section described the developed procedure for evaluating process alternatives based on the biorefinery concept. The method first jumbled the description of the features and simulation of proposed biorefinery designs. In this sense, relevant data is provided, including mass/energy balances,

production yields, energy usage, and downstream modeling, among others. The availability of this data allowed evaluating and further comparing simulated topologies under technical parameters and environmental assessment.

The analyzed biochemical pathways were modeled and simulated using Aspen.Plus[®] software package. As before mentioned, the mathematical formulation for performing an environmental assessment involved data about mass and energy balances, considering a baseline production capacity, which is fixed based on the availability of lignocellulosic wastes in the North Colombia region. The main assumptions for modeling and simulating the examined biorefinery designs are the followings:

- Steady-state modeling;
- Biomass is already cleaned and milled;
- All cellulose content is glucan;
- All hemicellulose content is xylan;
- All five-carbon carbohydrates are xylose;
- All six-carbon carbohydrates are glucose;
- Ash is assumed to be calcium oxide (CaO);
- Used microorganisms entered biological processes already available for hydrolysis and fermentation processes.

The procedure involved the conceptual design of production technologies based on biomass transformation. In this sense, topologies for the synthesis of ethanol, butanol, and succinic were simulated and further analyzed. Taking the data that provides a process simulation, this study implemented the WAR tool to evaluate the potential environmental effects derived from the steady-state operation of these plants. Additionally, technical parameters were considered to obtain more comprehensive insights from the developed procedure.

Two biorefinery designs were studied and compared based on data provided by the process simulation, estimation of technical parameters, and process evaluation under an environmental assessment. The first design, denominated as topology 1 focused on producing acetone, butanol, and ethanol via biomass fermentation. This design comprised of a feedstock feed flow of 12,809 t/y cassava waste, which is the primary raw material in this topology. The second biorefinery, denominated as topology 2, encompassed the production of ethanol and succinic acid via alcoholic fermentation. In this case, the feedstock feed comprised of a mixture of two biomasses; (i) cassava waste and (ii) banana rachis, with a flow of 7873.3 kg/h and 28,930.4 kg/h, respectively.

The chemical composition of lignocellulosic biomass is well established, mainly comprised of carbohydrates, moisture, acetate, and ash. Table 1 summarizes the corresponded mass fraction of constituent substances for cassava waste [20] and banana rachis [21].

Table 1. Chemical composition of lignocellulosic biomasses.

Component	Formula	Cassava Waste	Banana Rachis
Cellulose	C ₆ H ₁₀ O ₅	0.40	0.42
Hemicellulose	C ₅ H ₈ O ₄	0.13	0.13
Lignin	C _{7.3} H _{13.9} O _{1.3}	0.12	0.12
Water	H ₂ O	0.24	0.19
Ash	CaO	0.05	0.05
Acetate	[C ₂ H ₃ O ₂] ⁻	0.05	0.10

It is essential to describe that the feedstock flow assumed for these topologies corresponded to the local availability of these residues in the North Colombia region, specifically located in the department of Bolivar [22]. So, the biorefinery designs that were described in the following stages represent promising alternatives for waste valorization and adequate management of solid residues derived from the agroindustrial productive chain sector.

2.1. Topology 1: Butanol Production from Cassava Waste

The study presented here contemplated a topological pathway for the production of biobutanol from lignocellulosic biomass (cassava waste) through the biochemical pathway of acetone-butanol-ethanol (ABE) fermentation. The process comprised of four central stages: (a) pretreatment unit, (b) hydrolysis unit, (c) fermentation unit, and (d) purification unit. Globally, the process begins with the processing of raw material (lignocellulosic biomass) that entered the plant already cleaned and crushed. In this case, biomass was chemically treated to let obtaining solubilized five-carbon carbohydrates (xylose and arabinose) and cellulose [23]. Through filtration and separation stages, this section provides two main outlet streams (solid phase and liquid phase) that follow to hydrolysis and fermentation stages, respectively. It is worth mentioning that this study set the modified non-random two-liquid (NRTL) model and the Redlich–Kwong (RK) equation to model and estimate substance property and equilibria for this topology [24].

Solid-phase mainly composed of cellulose and not hydrolyzed carbohydrates, continued to a hydrolysis unit to solubilize six-carbon carbohydrates into glucose via enzymatic action [25]. The resulted stream from this operation was cleaned and sent to the fermentation stage, in which dissolved five and six-carbon sugars (xylose and glucose) were transformed into acetone, butanol, and ethanol, along with several byproducts, through biochemical reactions that involved the use of a specific microorganism [26]. ABE fermentation generated the main products in low concentration, so a complex separation/extraction system was included to obtain the products at commercial concentration and very high purity [27]. The following sections explain in a more detailed way all features and technical aspects about each of the described sections of the modeled butanol production process. Figure 1 displays the hierarchized butanol production layout that shows the main stages of the modeled process.

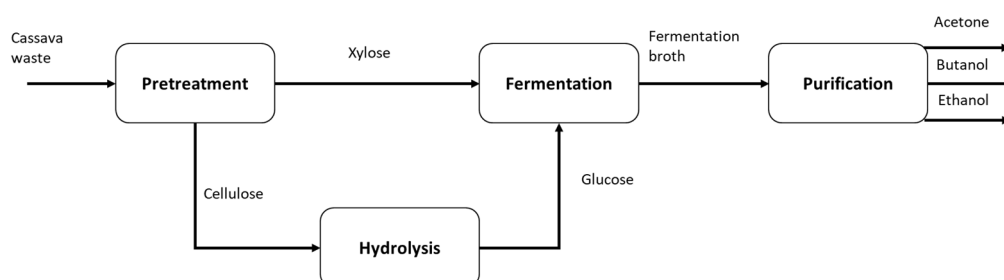


Figure 1. Hierarchized layout for butanol production.

2.1.1. Pretreatment Stage in Topology 1

As before mentioned, the pretreatment stage was the first section in the processing of topology 1. Figure 2 shows the process flowsheet of the pretreatment stage in topology 1. The dilute acid pretreatment was chosen as a chemical method for treating cassava waste in this topology. Biomass (stream 1) entered this subprocess already cleaned and milled, then to a mixing unit in which needed dilute H_2SO_4 , which remained below 0.5 wt % in the reactor, and was blended with the mainstream [28]. As the pretreatment reactor operated at 190 °C and 13 atm, the mixed biomass was preheated to 120 °C before entering the reactor, while the remaining energy and required pressure was supplied in the reactor by steam [29]. The dilute acid reactor broke the internal bonds of the biomass constituents, allowing the partial solubilization of glucose (7% from cellulose), xylose (90% from hemicellulose), acetic acid (100% from acetate), and a tiny portion of lignin (5%) [30].

The outlet stream was flash cooled to 1 atm, resulting in a decrease in the temperature of the system to 140 °C. The gas phase formed in the flash cooling (stream 8) was collected and condensed for sending this stream to the wastewater treatment. Otherwise, the mixed liquid and solid phase entered a filter unit, which separated the flow between cellulose and dissolved xylose. The process incorporated an ion-exchange unit (IEX-1) to reject acid substances in the rich-five carbon stream

for avoiding inhibitory and corrosion effects on the operation [31]. The EIX-1 unit operated at 40 °C and 1 atm and used ammonia (1 N) as an extractant agent during the operation of this stage [32]. This line of the process entered the overliming stage for further purification of the rich-xylose stream. The mainstream was first reacidified (MX-4) with sulfuric acid and subsequently neutralized (RX-2) with lime, precipitating gypsum ($\text{CaSO}_4 \times 2\text{H}_2\text{O}$) as the subproduct. A hydrocyclone unit separated liquid flow from formed gypsum and the remaining solids. In summary, the pretreatment stage processed the raw biomass, extracting xylose (stream 24) that was directed to the fermentation stage and cellulose (stream 14) that followed to the enzymatic hydrolysis stage.

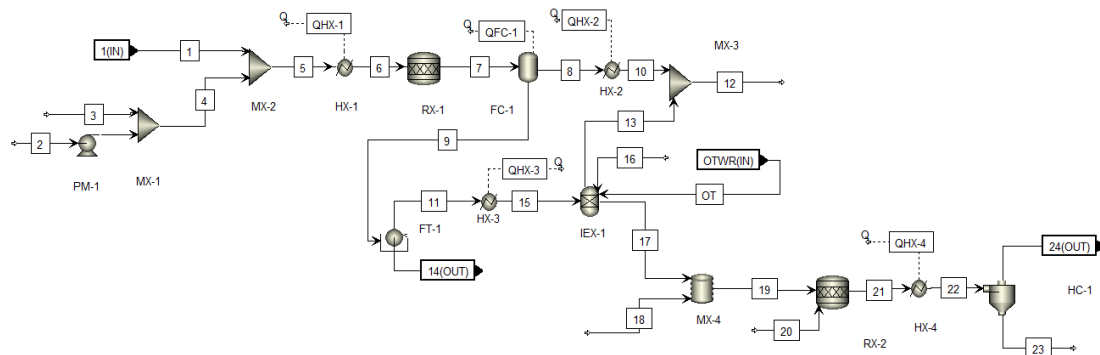


Figure 2. Pretreatment stage flowsheet in topology 1.

2.1.2. Hydrolysis Stage in Topology 1

As described, liquid–solid separation rejected solids from solubilized sugars, which were directly directed to ABE fermentation. A saccharification stage (RX-3) was added to transform cellulose into glucose through cellulase enzymatic action. In this case, the cellulase enzyme grouped a set of microorganisms, mainly comprised of endoglucanases, exoglucanases, and glucosidase, which broke the carbohydrate structure, its hydrolyzation, and further formation of glucose [33]. These enzymes were represented in the process by a cellulase flow (stream 30) that entered the RX-3 unit, allowing reducing sugar generation. The chemical formula ($\text{CH}_{1.57}$) used for the above substance was provided by [34] that reported a database for property estimation of missing components in biofuel processing using the Aspen Plus[®] software. Through the above processing, this system produced glucose from cellulose with a yield of 90%. The saccharification reactor operated at 30 °C and 1 atm, so the cellulose stream was cooled (HX-5) to needed reactor conditions, and lignin was extracted via filtration [35]. In this system, the water content needs to remain at 70 wt %, so stream 28 provided the demanded freshwater.

Furthermore, recycling stages were included to decrease water demand and raise glucose yield. Finally, a filtration unit (FT-5) removed impurities from the mainstream, and this was sent to the fermentation stage (stream 37). Figure 3 displays the process flowsheet of the hydrolysis section in topology 1.

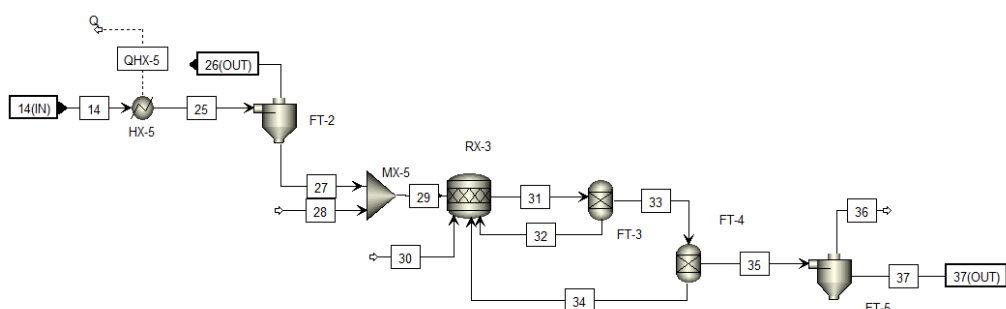


Figure 3. Hydrolysis stage flowsheet in topology 1.

2.1.3. Fermentation Stage in Topology 1

Stream with soluble sugars (glucose and pentose) were mixed before entering the ABE fermentation system. Both reducer sugars were converted in acetone, butanol, and ethanol through saccharolytic clostridia strain [36]. ABE fermentation (RX-4) was performed at 35 °C [37], under anaerobic conditions [38], and keeping water content above 80%, in which stream 40 supplied required water to meet this condition. Several chemical reactions and mechanisms occurred during the fermentation operation. Other side products like carbon dioxide, hydrogen (fermentation gases), acetic, and butyric acid, among others were produced [39]. It should be noted that there was also a generation of biomass accumulation that groups solid fermentation residues represented as cell biomass ($\text{CH}_{1.64}\text{O}_{0.39}\text{N}_{0.23}\text{S}_{0.0035}$) [40]. Figure 4 displays the process flowsheet of the fermentation stage in topology 1. In this work, this reaction system followed the configuration reported by Haigh et al. [41], which described that through continuous separate hydrolysis and fermentation, the system could reach production yields of 61.74% for butanol, 28.61% for acetone, and less than 1% for ethanol. It should be noted that butanol production was prioritized, so the selection of the ABE fermentation reaction configuration obeyed that goal. After this stage, the process continued to the separation unit for the extraction of desired products.

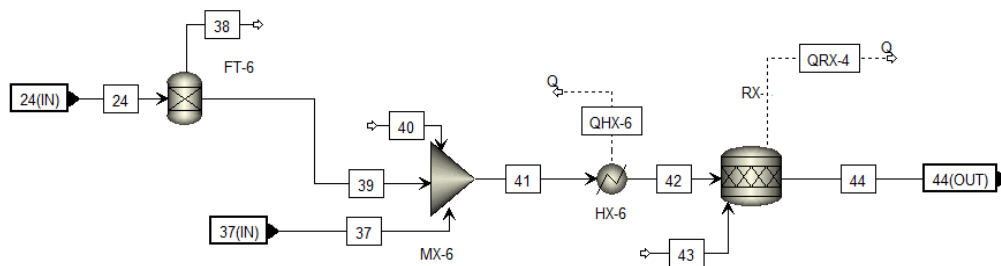


Figure 4. Fermentation stage flowsheet in topology 1.

2.1.4. Separation Stage in Topology 1

There are reported in the bibliography many methods and technologies to perform the extraction of ABE solvents [42]. These include gas stripping, azeotropic distillation, double-effect distillation, reactive distillation, filtration/membrane, and a combination of these technologies, among other types of downstream processing [43]. This work considered that a combination of gas stripping, double-effect distillation, and decantation unit could allow acceptable rates of product recovery, considering previous succeeded results [44]. In topology 1, the separation stage first encompassed a gas stripping operation (GS-1) that allowed the separation of most of the water content, along with impurities (stream 44). In this case, nitrogen was selected as a gas stripping agent [45]. As ABE products are volatile, these were trapped in the gas phases during gas stripping. Therefore, this stream was condensed to -10 °C and 1 atm (FC-2), allowing separation of fermentation gases and nitrogen (stream 48) from the solvents stream. The condensed stream was heated up to 25 °C and sent to the first double-effect distillation unit called the Beer Column (DT-1) [46]. In this unit, a massive amount of water was separated while ABE products out this unit in the distillate stream (stream 52). It is worth mentioning that the simulated DT-1 employed 15 separation stages, with a mass reflux ratio of 1.5 and condenser pressure of 1 atm. Figure 5 shows the process flowsheet for the separation stage in topology 1.

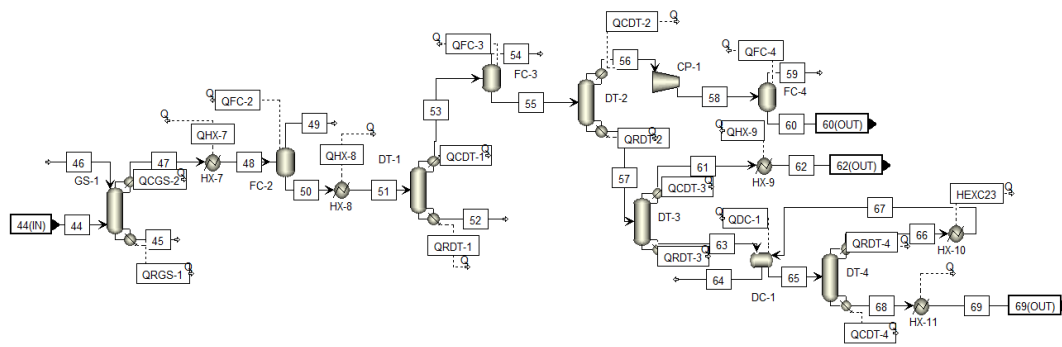


Figure 5. Separation stage flowsheet in topology 1.

A critical portion of remaining carbon dioxide was rejected through flash separation (FC-3), while the outlet liquid stream entered the second distillation tower denominated as the acetone column (DT-2). As its name might indicate, this separation unit permitted the extraction of acetone, which was the most volatile component between ABE solvents. The acetone column presented a configuration based on 15 equilibrium stages, a mass reflux ratio of 2.5, condensation pressure of 0.7 atm, and distillate rate of 740 kg/h. As a result, acetone was obtained in the distillate flow in DT-2, and it was sent to a compressor unit to raise the pressure back to atmospheric conditions. This design included a final flash separator (FC-4) in order to extract acetone (stream 59) at the highest possible purity. This product was obtained with a rate of 546.30 kg/h, with a mass concentration of 96.2%.

The bottoms stream of the acetone column (stream 56) entered a third double-effect distillation unit denominated ethanol column (DT-3). This tower comprised of the use of 25 stages, distillate flow of 280 kg/h, and mass reflux ratio of 10. This separation system used the difference in the boiling point between ethanol and butanol, obtaining the first one in the distillate flow. The current configuration of the ethanol column could just extract this substance at the azeotrope concentration that it forms with water [47]. This purity corresponded to 85.1 wt % ethanol. Higher ethanol purities can be obtained by implementing different specific separation technologies; these can include azeotropic distillation, reactive distillation, and molecular sieves, among others [47]. This work did not include additional purification equipment for ethanol extraction since this substance is considered as a subproduct of the process. Table 2 summarizes the stoichiometric equations of simulated stages and their corresponding reactions for topology 1.

Table 2. Summary of the stoichiometric equations for topology 1.

Stage	Reaction	Yield	Ref.
Pretreatment	Glucan + H ₂ O → Glucose	0.07	[34]
	Xylan + H ₂ O → Xylose	0.90	
	Xylan → Furfural + 2H ₂ O	0.05	
	Acetate → Acetic acid	1.00	
	Lignin → Soluble lignin	0.05	
Enzymatic hydrolysis	Glucan + H ₂ O → Glucose	0.90	[30]
ABE fermentation	Glucose → Butanol + 2CO ₂ + H ₂ O	0.50	[48]
	Glucose + H ₂ O → Acetone + 3CO ₂ + 4H ₂	0.28	
	Glucose → 2Ethanol + 2CO ₂	0.05	
	Glucose → Butyric acid + 2CO ₂ + 2H ₂	0.10	
	Glucose → 3 Acetic acid	0.07	
	6Xylose → 5Butanol + 10CO ₂ + 5H ₂ O	0.50	
	Xylose → Acetone + 2CO ₂ + 2H ₂	0.30	
	3Xylose → 5Ethanol + 5CO ₂	0.15	
2Xylose → 5 Acetic acid	0.01		

Most of the butanol flow remained in the bottoms stream (stream 62) of the ethanol column; this stream was directed to a decanter unit in order to break the heterogeneous azeotrope that was formed between butanol and water. Decantation operation (DC-1) was developed at 60 °C and 0.7 atm, which separated the main flow between the rich-aqueous stream (stream 63) and rich-organic stream (stream 64). The last one, with the majority of butanol flow, was sent to a final distillation column (DT-4) to extract this product at very high purity. This distillation tower is called the butanol column. The configuration of this unit involved setting eight stages, a mass reflux ratio of 2, and a distillate rate of 670 kg/h. It is worth highlighting that the process included recycling of distillation flow (stream 65) to increase butanol yield. The butanol column allowed separation of persisting impurities and water content, obtaining a butanol product flow of 1304.70 kg/h with a concentration of almost 97%. All technical information about separation units for topology 1 are reported in Table 3. Table 4 summarizes process data about main streams in simulated topology 1.

Table 3. Summary of the technical parameters of the main separation units in topology 1.

Unit	Operation	Reaction	Value
GS-1	Gas stripping	Number of stages	8
		Reflux ratio	1.5
		Condenser	Partial-vapor
		Feed stage	2
		Gas-feed stage	7
		Condenser pressure	1 atm
DT-1	Double-effect distillation	Number of stages	15
		Reflux ratio	1.5
		Condenser	Partial-vapor
		Feed stage	2
		Distillate rate	3793 kg/h
		Condenser pressure	1 atm
DT-2	Double-effect distillation	Number of stages	15
		Reflux ratio	2.5
		Condenser	Partial-vapor
		Feed stage	7
		Distillate rate	740 kg/h
		Condenser pressure	0.7 atm
DT-3	Double-effect distillation	Number of stages	25
		Reflux ratio	10
		Condenser	Partial-vapor
		Feed stage	7
		Distillate rate	280 kg/h
		Condenser pressure	0.3 atm
DT-4	Double-effect distillation	Number of stages	8
		Reflux ratio	2
		Condenser	Partial-vapor
		Feed stage	4
		Distillate rate	670 kg/h
		Condenser pressure	0.5 atm

Table 4. Process data of the main streams for topology 1.

Variable	1	24	37	42	44	60	62	69
Temperature (°C)	28.00	50.0	30.4	35.0	35.0	35.0	30.0	28.0
Pressure (bar)	1.01	1.0	1.0	1.0	1.0	1.0	1.0	1.0
Enthalpy Flow (Gcal/h)	−26.81	−3.7	−93.4	−154.1	−161.0	−0.6	−0.5	−1.5
Mole Flows (kmol/h)	240.74	71.5	1371.2	2261.7	2483.1	9.7	7.3	18.9
Mass Flows (kg/h)	12,809	2910	29,871	47,584	49,084	546.3	280.0	1305
Mass fraction of components								
Water	0.174	0.131	0.750	0.803	0.803	0.008	0.136	0.024
Lignin	0.141	0.025	0.000	0.000	0.000	0.000	0.000	0.000
Cellulose	0.435	0.000	0.000	0.000	0.000	0.000	0.000	0.000
Hemicellulose	0.141	0.000	0.000	0.000	0.000	0.000	0.000	0.000
Ash	0.054	0.191	0.000	0.000	0.000	0.000	0.000	0.000
Xylose	0.000	0.507	0.000	0.031	0.001	0.000	0.000	0.000
Ethanol	0.000	0.000	0.000	0.000	0.005	0.024	0.851	0.000
Glucose	0.000	0.000	0.174	0.000	0.000	0.006	0.000	0.000
Cell biomass	0.000	0.000	0.000	0.000	0.056	0.000	0.000	0.000
Calcium hydroxide	0.000	0.119	0.000	0.117	0.000	0.000	0.000	0.000
Acetic acid	0.000	0.000	0.000	0.000	0.010	0.000	0.000	0.000
Acetate	0.054	0.000	0.000	0.000	0.000	0.000	0.000	0.000
Carbon Dioxide	0.000	0.000	0.000	0.000	0.074	0.005	0.000	0.000
Butanol	0.000	0.000	0.000	0.000	0.030	0.000	0.013	0.964
Acetone	0.000	0.027	0.000	0.002	0.014	0.962	0.000	0.000
Hydrogen	0.000	0.000	0.000	0.000	0.002	0.000	0.000	0.000
Butyric acid	0.000	0.001	0.000	0.000	0.005	0.000	0.000	0.011

2.2. Topology 2: Ethanol and Succinic Acid Production from Banana Rachis and Cassava Waste

This study considered the evaluation of a second topological pathway for the production of succinic acid and ethanol from a biomass mixture composed of banana rachis and cassava waste. The process comprised of five central stages: (a) pretreatment unit, (b) hydrolysis unit, (c) five carbon fermentation, (d) six carbon fermentation, and (e) purification unit. Figure 6 displays the generalized process layout for topology 2. Likewise, topology 2 was first stated with the treatment of raw material employing dilute acid technology in order to break and solubilize constituent carbohydrates presented in the molecular structure of the biomass.

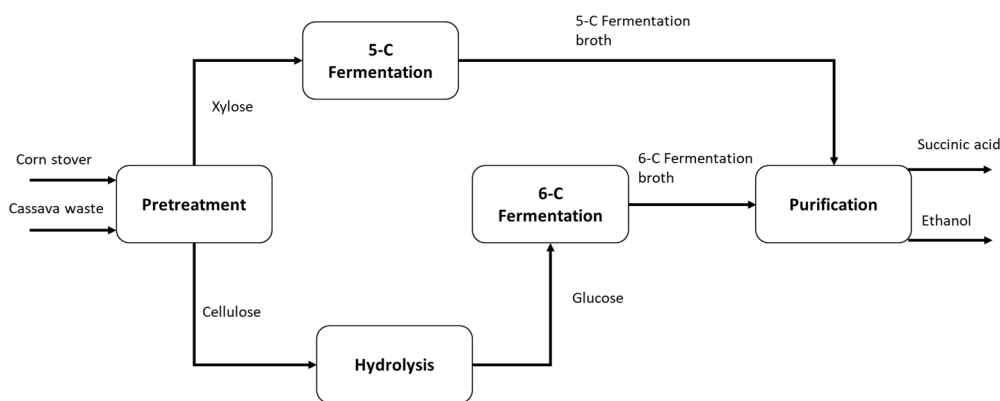


Figure 6. Hierarchized layout for succinic acid and ethanol production.

The main flow in the pretreatment stage was divided into the liquid stream (mainly xylose) and solid stream (mainly glucose). The first one was directly directed to the five-carbon fermentation stage

for ethanol production [49]. Otherwise, the solid stream with non-dissolved cellulose was sent to the hydrolysis unit for glucose formation via enzymatic action. The outlet stream from the hydrolysis section entered the six-carbon fermentation unit in order to produce succinic acid as the main product and acetic acid as a byproduct through biological processes [30]. Both leaving streams from the fermentation processes were sent to the purification stage in order to extract succinic acid and ethanol at high purity concentration. The following sections explain more technical details associated with the modeling and simulation of the described pathway for succinic acid and ethanol coproduction. In this case, the NRTL method was selected as the thermodynamic model for property estimation considering recommendations made by the National Renewable Energy Laboratory (NREL) and its reported Aspen Database for estimation of biofuel processing substances [34].

2.2.1. Pretreatment Stage in Topology 2

This stage was designed and simulated, considering the same conditions described for topology 1. The main difference for this case was that topology 2 processes a mixture of two raw materials (stream 1 and stream 2), which were chemically treated via the acid dilute pretreatment. Figure 7 displays the pretreatment stage in topology 2. Additionally, the conditions of the pretreatment reactor (190 °C and 13 atm) and further flash cooling, filtration, and overliming were the same settings for the ABE fermentation process. The rich cellulose stream (stream 15) was obtained in the first filtration unit, while the separated liquid phase followed to the ion-exchange unit (IEX-1) for the rejection of acid substances and further reacidification (MX-5) and overliming stages (RX-2). A hydrocyclone (HC-1) split gypsum formed during overliming, and the purified liquid stream with xylose was sent to the five-carbon fermentation unit. Otherwise, stream 15 was directed to the enzymatic hydrolysis stage for cellulose saccharification.

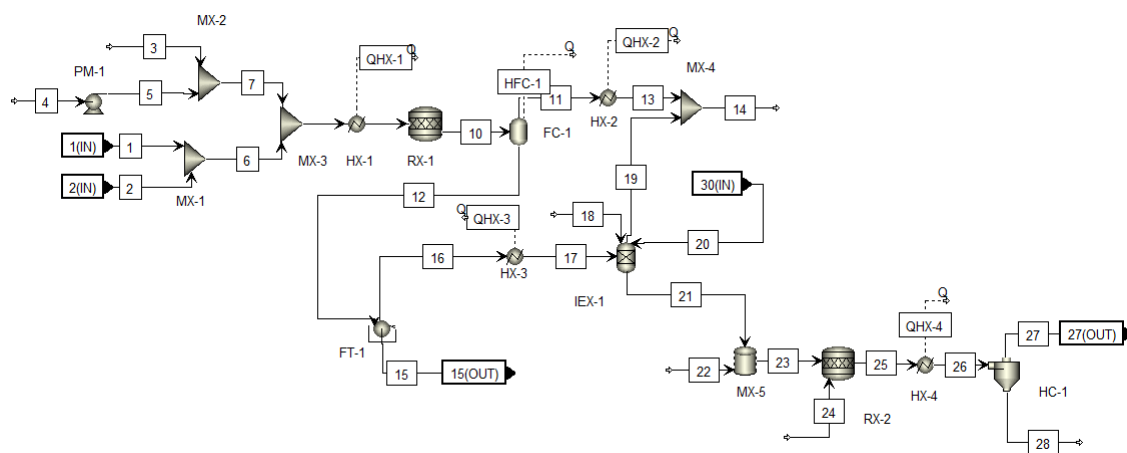


Figure 7. Pretreatment stage flowsheet in topology 2.

2.2.2. Hydrolysis Stage in Topology 2

As explained for topology 1, the most crucial aspect of hydrolysis is the possibility to obtain glucose from cellulosic material using a cellulase enzyme. As mentioned for the previous section, the enzymatic hydrolysis section in topology 2 presented the same setting and features implemented for this section in topology 1. In this case, the inlet flow of this stage was stream 15 (with cellulose content) that was cooled (HX-5) to the required temperature for performing hydrolysis reaction. Stream 32 supplied the needed water to keep the biological system under demanded moisture content. Recycling stages (FT-3 and FT-4) were included to increase the cellulose production rate. This processing was a crucial stage since higher production of glucose gives the possibility to generate higher amounts of succinic acid. A filter rejected impurities in the mainstream, so the filtered glucose flow (stream 41) was directed to the six-carbon fermentation unit. Figure 8 shows the process flowsheet of the hydrolysis section in topology 2.

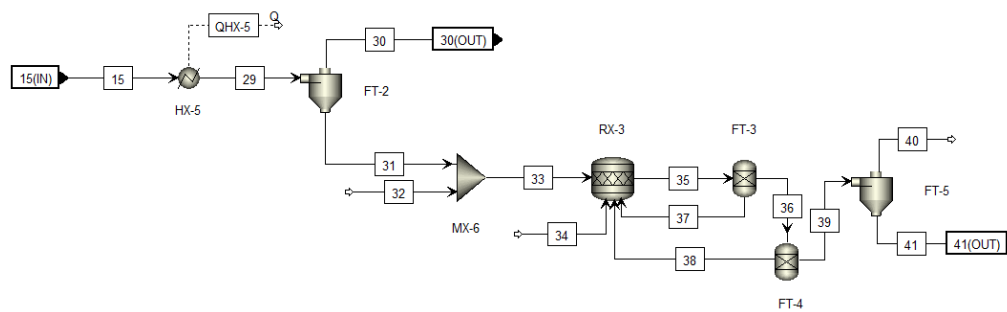


Figure 8. Hydrolysis stage flowsheet in topology 2.

2.2.3. Five-Carbon Fermentation in Topology 2

Liquid stream coming from the pretreatment section entered this unit (as main inlet flow) with a mixture of five-carbon sugars mainly composed of xylose. This stream entered a first filtration unit to remove remaining impurities in the flow that might implicate inhibitory effects in the fermentation system. The development of the fermentation system for this stage involves a variety of bioprocesses and bioreactions in the reactor that allow conversion of reducer sugars to ethanol, glycerol, lactic acid, and carbon dioxide, among others components [50]. This study selected the biocatalyst *Zymomonas mobilis*, which is a promising microorganism for procuring ethanol production via fermentation [51]. Figure 9 displays the process flowsheet of five-carbon fermentation in topology 2.

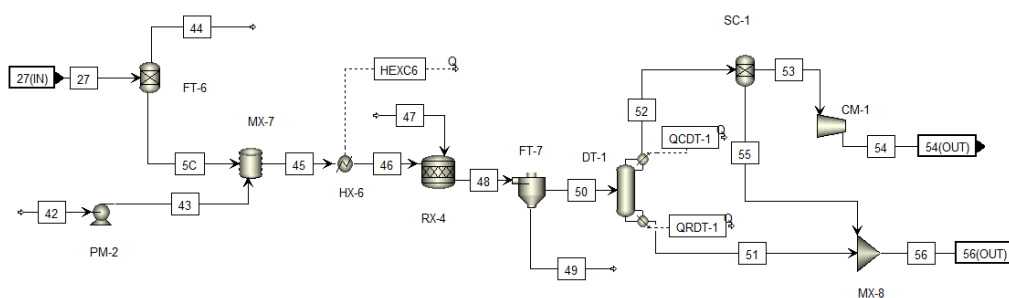


Figure 9. Five-carbon fermentation flowsheet in topology 2.

In this topology, the fermentation reactor (RX-4) operated at 30 °C and 1 atm, maintaining water content of 80 wt %. Fermentation reactions demand water content to reach optimum conditions that, in this case, stream 42 supplied needed freshwater. The system involved several reactions in which xylose was transformed into ethanol, glycerol, xylitol, and acetic and lactic acids, among others. Additionally, fermentation gases like oxygen, hydrogen, and carbon dioxide were generated during this operation [52], and the chemical equations and reactions used in this simulated took into account the generation of solid residues derived from the fermentation system [30,53]. Furthermore, production selectivity for these reactions, through the action of *Zymomonas mobilis* (supplied through stream 47), corresponded to a yield of 85% for ethanol, 0.3% for glycerol, 1.4% for acetic acid, and 0.2% for lactic acid [30].

The fermentation broth (stream 48) generated from the reaction system was sent to filtration (FT-7) for the removal of impurities and pollutants (stream 49). The filtered stream entered the beet column (DT-1) for rejecting CO₂ dissolved in the fermentation broth and a massive amount of water. This unit was quite vital since ethanol was present in the mixture, with a concentration below 8%. Distillate flow (stream 52) leaving the beer column was sent to a water scrubber (SC-1), recovering a portion of the dissolved ethanol (stream 55) mixed with carbon dioxide in the fermentation vent stream. It is worth mentioning that stream 55 and stream 51 were mixed (MX-8) and sent to the purification stage in order to produce highly concentrated ethanol. Otherwise, scrubbed carbon dioxide (stream 53) was compressed (CM-1) and sent to the six-carbon fermentation unit for CO₂ supply, decreasing the rate

of fresh supply for this reagent. The described configuration not only could permit to reduce the operating cost of the plant but also meant a generation of less environmental impacts, decreasing the carbon footprint of the process [54].

2.2.4. Six-Carbon Fermentation Stage in Topology 2

Fermentation of glucose involved the additions of a specialized biocatalyst for producing succinic acid from this substance. There is a set of studied microorganisms that can be used for the fermentation of both five and six-carbon sugars. Some advantages and disadvantages of them are associated with their productivity, stability, and selectivity [55]. For the fermentation of glucose to form succinic acid (and acetic acid), the recombinant *C. glutamicum* was selected since through this biocatalyst, the fermentation system can reach succinic acid about 0.149 kg/L under anaerobic conditions and carbon dioxide atmosphere [30]. Considering these conditions, the fractional conversion yield of glucose to succinic acid was 0.70 kg/kg, while this parameter corresponded to 0.10 kg/kg for acetic acid. Stream 41 (xylose and water mixture) entered a flash separator (FC-2) that operated above 100 °C, and 1 atm, for exceeding water removal and persisting impurities in the stream.

Figure 10 shows the process flowsheet diagram for the six-carbon fermentation in topology 2. The flashed stream continued to a heat exchange unit (HX-7) to decrease the temperature back to 30 °C before entering the six-carbon fermentation system (RX-5). As before mentioned, this reaction mechanism coproduces succinic acid and acetic acid, employing the recombinant *C. glutamicum* under 30 °C and 1 atm. It should be noted that succinic acid parted from the reaction between glucose and carbon dioxide. The last one is partially supplied through the integration of stream 54 that came from the scrubber unit in the five-carbon fermentation section.

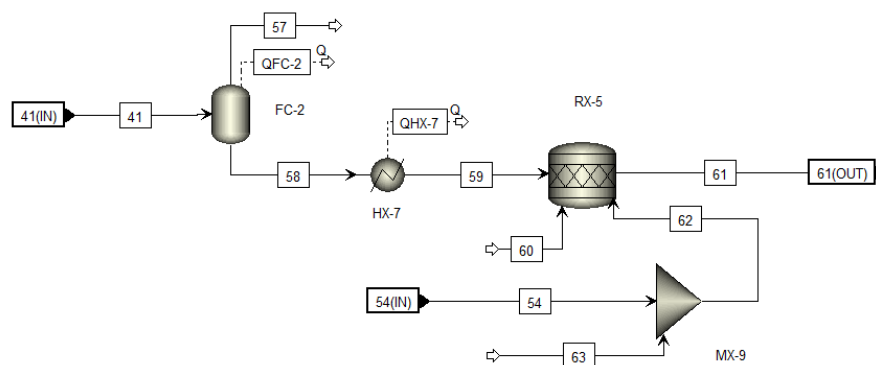


Figure 10. Six carbon fermentation flowsheet in topology 2.

2.2.5. Purification Stage Flowsheet in Topology 2

Purification unit for topology 2 involved the treatment and extraction of both the main products (succinic acid and ethanol), which were generated, at a shallow concentration, in performed fermentation stages. In this case, stream 56 (leaving 5-C fermentation) and stream 61 (leaving 6-C fermentation) were the main feed flows with the desired products that needed to be extracted. Stream 56 with ethanol content was sent to a second distillation unit (DT-2) to separate ethanol from water content. DT-2 operated, taking 14 equilibrium stages, a mass reflux ratio of 5, and a condenser pressure of 1 atm. It is worth mentioning that this operation permitted to obtain ethanol at the azeotrope concentration, so an additional molecular sieve adsorption (MS-1) unit was included in this design for reaching higher ethanol purity. MS-1 operated considering a temperature of 60 °C and a mass flow supply of carbon dioxide (stream 85) with a pressure of 200 psig [47]. Thus, high concentrated ethanol (stream 83) was produced with a concentration of 99.99 wt % and mass flow of 2277.90 kg/h. Table 5 summarizes data about main streams in topology 2.

Table 5. Process data of the main streams for topology 2.

Variable	1	2	15	27	46	59	76	83
Temperature (°C)	28	28	166.85	50	30	30	4	28
Pressure (bar)	1.01	1.01	1.01	1.01	1.01	1.01	1.01	1.01
Enthalpy Flow (Gcal/h)	-16.79	-61.38	-39.59	-13.43	-99.2	-295.04	-13.14	-3.3
Mole Flows (kmol/h)	155.56	552.09	220.47	246.21	1,451.99	4,300	129.1	49.48
Mass Flows (kg/h)	7873.3	28,930.4	23,842.2	10,350.6	30,824.3	92,043.7	13,865.7	2277.9
Water	0.189	0.174	0.009	0.121	0.827	0.776	0.018	0.000
Lignin	0.119	0.141	0.205	0.024	0.000	0.000	0.000	0.000
Cellulose	0.417	0.435	0.619	0.000	0.000	0.000	0.000	0.000
Hemicellulose	0.129	0.141	0.011	0.000	0.000	0.000	0.000	0.000
Ash	0.047	0.054	0.036	0.187	0.001	0.000	0.000	0.000
Xylose	0.000	0.000	0.096	0.502	0.135	0.000	0.000	0.000
Ethanol	0.000	0.000	0.000	0.000	0.000	0.000	0.000	1.000
Glucose	0.000	0.000	0.023	0.119	0.032	0.161	0.000	0.000
Furfural	0.000	0.000	0.000	0.001	0.000	0.000	0.000	0.000
Sulfuric acid	0.000	0.000	0.001	0.000	0.000	0.000	0.000	0.000
Gypsum	0.000	0.000	0.000	0.027	0.000	0.000	0.000	0.000
Calcium hydroxide	0.000	0.000	0.000	0.019	0.005	0.000	0.000	0.000
Acetic acid	0.000	0.000	0.001	0.000	0.000	0.000	0.000	0.000
Succinic acid	0.000	0.000	0.000	0.000	0.000	0.000	0.982	0.000
Cellulase	0.000	0.000	0.000	0.000	0.000	0.062	0.000	0.000
Acetate	0.099	0.054	0.000	0.000	0.000	0.000	0.000	0.000

Figure 11 displays the process flowsheet of the purification stage in topology 2. The other process line in this section involved the separation of succinic acid. This purification step was developed from the formation of sodium succinate. Succinic acid was put in contact (RX-6) with lye (stream 62), forming a solution composed of ion succinate, H₂O, and Na⁺. This stream (stream 63) was evaporated for the removal of water, acetic acid, and other impurities, and sent to a second reaction system (RX-7) in which succinic acid was reformed by adding sulfuric acid. The mechanism involved sodium sulfate generation taking Na⁺ and sulfate group in sulfuric acid, and the formation of succinic acid through interaction between solubilized succinate group and protons (H⁺) donated by sulfuric acid [56]. Table 6 reports the technical parameters of the main separation units of topology 2.

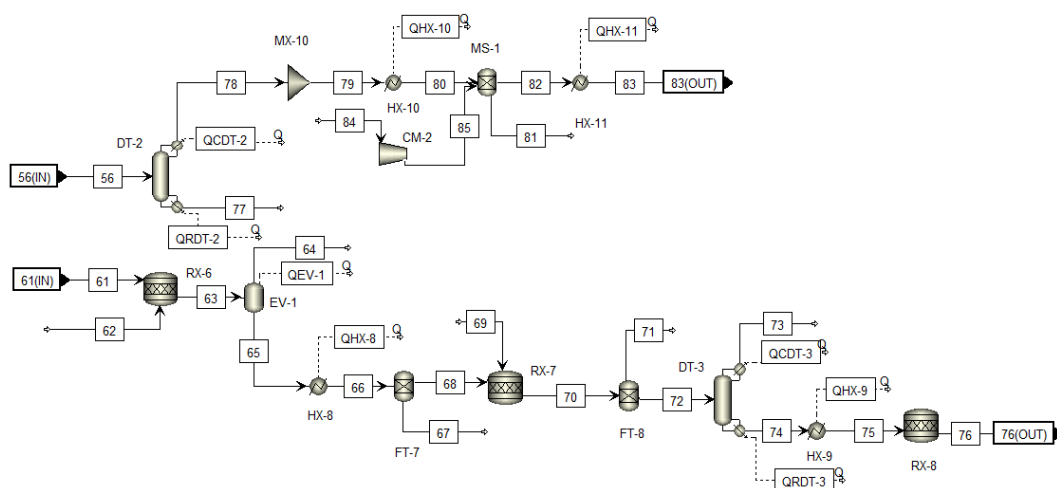


Figure 11. Purification stage flowsheet in topology 2.

Table 6. Summary of the technical parameters of the main separation units in topology 2.

Unit	Operation	Reaction	Value	
DT-1	Double-effect distillation	Number of stages	6	
		Reflux ratio	1.5	
		Condenser	Partial-Vapor	
		Feed stage	2	
		Distillate rate	2800 kg/h	
			Condenser pressure	1 atm
DT-2	Double-effect distillation	Number of stages	14	
		Reflux ratio	5	
		Condenser	Partial-Vapor	
		Feed stage	7	
		Distillate rate	2650 kg/h	
			Condenser pressure	1 atm
DT-3	Double-effect distillation	Number of stages	7	
		Reflux ratio	1.5	
		Condenser	Partial-Vapor	
		Feed stage	2	
		Distillate rate	950 kg/h	
			Condenser pressure	

The above procedure is needed because direct distillation does not guarantee successful separation of the not desired component that allows obtaining succinic acid at an analytical degree. The outlet stream from RX-7 (stream 70) passed through filtration (FT-8) for the removal of lye and sodium sulfate (solid components), and continued to the vacuum distillation unit (DT-3) allowing for water removal. Finally, the bottoms stream of vacuum distillation was cooled (HX-9) and crystallized (RX-8) under 4 °C, obtaining the product with a purity of 98.2% and mass flow rate of 13,865.7 kg/h [57]. Table 7 summarizes the stoichiometric equations of simulated stages and their corresponding reactions for topology 1.

Table 7. Summary of the stoichiometric equations of the main stages for topology 2.

Stage	Reaction	Yield	Ref.
Pretreatment	$\text{Glucan} + \text{H}_2\text{O} \rightarrow \text{Glucose}$	0.07	[32]
	$\text{Xylan} + \text{H}_2\text{O} \rightarrow \text{Xylose}$	0.90	
	$\text{Xylan} \rightarrow \text{Furfural} + 2\text{H}_2\text{O}$	0.05	
	$\text{Acetate} \rightarrow \text{Acetic acid}$	1.00	
	$\text{Lignin} \rightarrow \text{Soluble lignin}$	0.05	
Enzymatic hydrolysis	$\text{Glucan} + \text{H}_2\text{O} \rightarrow \text{Glucose}$	0.90	
C5 Fermentation	$3\text{Xylose} \rightarrow 2 \text{ ethanol} + 2\text{CO}_2$	0.85	[30]
	$3\text{Xylose} + 5\text{H}_2\text{O} \rightarrow 5\text{Glycerol} + 2.5\text{O}_2$	0.003	
	$3\text{Xylose} + 5\text{CO}_2 \rightarrow 5\text{Succinic acid} + 2.5\text{O}_2$	0.009	
	$2\text{Xylose} \rightarrow 5\text{acetic acid}$	0.014	
	$3\text{Xylose} \rightarrow 5\text{lactic acid}$	0.002	
	$\text{Glucose} \rightarrow 2 \text{ ethanol} + 2\text{CO}_2$	0.95	
	$\text{Glucose} + 2\text{H}_2\text{O} \rightarrow 2\text{Glycerol} + \text{O}_2$	0.004	
	$\text{Glucose} + 2\text{CO}_2 \rightarrow 2\text{Succinic acid} + \text{O}_2$	0.006	
	$\text{Glucose} \rightarrow 3\text{acetic acid}$	0.015	
$\text{Glucose} \rightarrow 2\text{lactic acid}$	0.02		
C6 Fermentation	$\text{Glucose} + 2\text{CO}_2 \rightarrow 2\text{succinic acid} + \text{O}_2$	0.70	
	$\text{Glucose} \rightarrow 3\text{acetic acid}$	0.10	
	$3\text{Xylose} \rightarrow 5\text{Ethanol} + 5\text{CO}_2$	0.15	
	$2\text{Xylose} \rightarrow 5 \text{ Acetic acid}$	0.01	

2.3. Process Evaluation under an Environmental Assessment

This study addressed the implementation of process evaluation via an environmental assessment to examine two promising alternatives for the production of biofuels and chemical derivatives from lignocellulosic biomass. This work selected the waste reduction algorithm to develop an environmental impact evaluation of examined bioprocess topologies. This selection obeyed the fact that this algorithm is freely available to download on the web page of the United States Environmental Protection Agency (USEPA) through the WAR GUI software[®] [58]. This tool is implemented to estimate environmental impact generation derived from a physical–chemical process.

The WAR methodology introduced the potential environmental impact (PEI) concept, which measures the possible effects on the environment due to an accidental discharge or emission over an ecosystem [59]. These impacts are evaluated from both mass and energy streams. The procedure of the WAR method involved estimating eight impact categories classified between atmospheric and toxicological categories [60]. Table 8 provides information about the evaluated categories in the WAR.

Table 8. Description of the impact categories in waste reduction algorithm (WAR).

Category	Symbol	Equation
Toxicological		
Human toxicity by ingestion	HTPI	$HTPI = \frac{1}{LD_{50}}$
Human toxicity by dermal exposure	HTPE	$HTPE = \frac{1}{TLV}$
Aquatic toxicity potential	ATP	$HTPE = \frac{1}{LC_{50}}$
Terrestrial toxicity potential	TTP	$TTP = \frac{1}{LD_{50}}$
Atmospherical		
Global warming potential	GWP	$GWP = \frac{\int a_i c_i(t) dt}{\int a_{CO_2} c_{CO_2}(t) dt} m_i$
Ozone depletion potential	ODP	$ODP = \frac{\delta[O_3]_i}{\delta[O_3]_{FCKW-11}} m_i$
Photochemical oxidation potential	PCOP	$PCOP = \frac{b_i(t)}{a_{C_2H_4}} m_i$
Acidification potential	AP	$AP = \frac{V_i}{V_{SO_2}} \frac{M_i}{M_{SO_2}} m_i$

The application of equations shown in Table 8 was attained with the data about extended mass (m_i is the mass flow of component i) and energy balance of the analyzed process. These also considered the calculation of other side indicators that included a rat oral lethal dose at 50% (LD_{50}), threshold limit value (TLV), lethal concentration at 50% in water (LC_{50}), a_i radiation heat absorption per unit GHG i , a_{CO_2} represents the same absorption but in terms of CO_2 , $c_i(t)$ is the gas concentration of GHG time-basis, and $c_{CO_2}(t)$ is the same concentration in terms of CO_2 . Besides, the ozone depletion potential (ODP) was calculated in kilograms of CFC-11 equivalent, where $\delta[O_3]_i$ refers to the global ozone depletion produced by one unit of gas i , $\delta[O_3]_{FCKW-11}$ is the depletion of ozone produced by a unit of CFC-11, and m_i is the mass (kg) of the gas emitted. The photochemical oxidation potential (PCOP; kg C_2H_4 -equiv.) involves the change in ozone concentration due to a change in the emission of a volatile organic compound i , $a_{C_2H_4}$ refers to this same change, but with respect to ethylene emission, $b_i(t)$ is the integrated emission of a volatile organic compound i up to a time t , $b_{C_2H_4}(t)$ refers to this last condition with respect to ethylene, and m_i is the mass (kg) of the organic compound volatile emitted. Finally, the acidification potential (AP) category (kg SO_2 -equiv.) implicated calculation of the acidification potential, where V_i is the acidification potential of component i , V_{SO_2} is the acidification potential of SO_2 , and M_{SO_2} is the unit mass of SO_2 . WAR for estimating environmental impacts uses

four indicators considering the defined boundaries of the system. Equations (1)–(4) provides the mathematical expression to calculate these environmental impact indicators [61].

$$i_{out}^{(t)} = i_{out}^{(cp)} + i_{out}^{(ep)} + i_{we}^{(cp)} + i_{we}^{(ep)} = \sum_j^{cp} M_j^{(out)} \sum_k^{cp} X_{kj} \psi_k + \sum_j^{ep-g} M_j^{(out)} \sum_k^{ep-g} X_{kj} \psi_k \quad (1)$$

$$i_{out}^{(t)} = \frac{\left(i_{out}^{(cp)} + i_{out}^{(ep)} + i_{we}^{(cp)} + i_{we}^{(ep)} \right)}{\sum_P P_P} = \frac{\sum_j^{cp} M_j^{(out)} \sum_k^{cp} X_{kj} \psi_k + \sum_j^{ep-g} M_j^{(out)} \sum_k^{ep-g} X_{kj} \psi_k}{\sum_P P_P} \quad (2)$$

$$i_{gen}^{(t)} = i_{out}^{(cp)} - i_{in}^{(cp)} + i_{out}^{(ep)} - i_{in}^{(ep)} + i_{we}^{(cp)} + i_{we}^{(ep)} \\ = \sum_j^{cp} M_j^{(out)} \sum_k^{cp} X_{kj} \psi_k - \sum_j^{cp} M_j^{(in)} \sum_k^{cp} X_{kj} \psi_k + \sum_j^{ep-g} M_j^{(out)} \sum_k^{ep-g} X_{kj} \psi_k \quad (3)$$

$$i_{gen}^{(t)} = \frac{i_{out}^{(cp)} - i_{in}^{(cp)} + i_{out}^{(ep)} - i_{in}^{(ep)} + i_{we}^{(cp)} + i_{we}^{(ep)}}{\sum_P P_P} \\ = \frac{\sum_j^{cp} M_j^{(out)} \sum_k^{cp} X_{kj} \psi_k - \sum_j^{cp} M_j^{(in)} \sum_k^{cp} X_{kj} \psi_k + \sum_j^{ep-g} M_j^{(out)} \sum_k^{ep-g} X_{kj} \psi_k}{\sum_P P_P} \quad (4)$$

Equation (1) provides the expression for the output rate of PEI, Equation (2) gives the mass output rate, Equation (3) the total generation rate of PEI, and the total mass generation rate is estimated through Equation (4). In this sense, $i_{out}^{(cp)}$ and $i_{in}^{(cp)}$ are the leaving and entering velocities of PEI derived from chemical interactions within process boundaries, respectively. Otherwise, $i_{out}^{(ep)}$ and $i_{in}^{(ep)}$ provide the rate of PEI leaving and entering the system due to energy generation within the process. $i_{we}^{(ep)}$ and $i_{we}^{(cp)}$ are the indicators for leaving PEI rates from the process as a consequence of waste energy release derived from energy generation and chemical stages throughout the process boundaries. P_p is the mass flow rate of product p , mass flow input and output of a stream j are represented by $M_j^{(in)}$ and $M_j^{(out)}$, respectively, X_k is the mass fraction of a chemical compound k in the stream j , and ψ_k is the overall PEI of substance k [31].

In this section, analysis results are presented, including an environmental assessment and a comparison of technical parameters for the simulated topologies. It is worth highlighting that the developed assessment focused on the analysis of a bounded system delimited by its process and energy streams. As the goal of the algorithm is to minimize the PEI for a process instead of minimizing the amount of waste (pollutants) generated by a process; the analysis presented here only included the manufacturing section.

3. Results and Discussion

Process simulation and analysis were performed, considering the described topologies in the methodology section. In this sense, this work analyzed a biobutanol production via ABE fermentation and a bioprocess for bioethanol/succinic acid synthesis via alcoholic fermentation. One of the essential features of process simulation is that this tool can provide several data about the performance of a physical–chemical process, parting from property estimation, thermodynamic equilibria, modeling downstream processing, and generation of extended mass and energy balances, among others [62]. So, it is advantageous to implement computer-aided modeling and simulation for performing a comparison of process topologies, seeking the most suitable design based on engineering and decision-making criteria.

3.1. Results of Technical Performance Indicators

The first part of the developed analysis included the estimation of technical parameters in order to compare the process performance of evaluated topologies. Likewise, variables like energy consumed, product yield, material consumption, water consumption, total product flow, and resource energy

efficiency were considered in the analysis. Table 9 summarizes the results of evaluated technical parameters for both Topology 1 and Topology 2.

Table 9. Technical parameters for the evaluated topologies.

Technical Parameter	Topology 1	Topology 2
Energy consumed (GJ/h)	525.27	1138.76
Resource energy efficiency (%)	12.38	20.43
Product(s) Yield (%)	16.64	43.86
Total product flow (kg/h)	2130.99	16,143.67
Total material consumption (kg)	120,150.04	284,758.03
Total water consumption (m ³ /h)	74,628.70	221,398.02

According to the data reported in Table 9, topology 2 demanded more energy in its processing than topology 1, to generate the desired production. This difference represents an increase of 116.79% with respect to the first topology. It should be mentioned that this is an expected value since topology 2 had a higher raw material processing capacity (36,803.7 kg/h) than that modeled for topology 1 (12,808.60 kg/h); this might indicate that topology 2 handled a more substantial mass inventory than topology 1. So, the analysis was included in the evaluation of resource energy efficiency to overcome the limited data that the energy consumption indicator provided. Equation (5) shows the expression to estimate this parameter [63].

$$\text{Resource energy efficiency (\%)} = \frac{\text{Energy content of product}}{\text{Total input energy}} \quad (5)$$

In this sense, the resource energy efficiency resulted in a higher value for topology 2 compared with the obtained result for topology 1. These outcomes indicate that even though topology 2 demanded higher energy usage, this processing pathway better used its available resources, meaning it had better energy performance compared with topology 1. Moreover, it should be noted that both topologies showed a low performance for this indicator since it is expected that a process based on biofuel production should obtain resource energy efficiencies near to 100%. Otherwise, it is worth mentioning that the total energy content of products is the sum of the specific energy content of each substance plus its mass flow. Ethanol has an energy content of 0.20 GJ/kg, while this parameter for butanol was 0.33 GJ/kg, for acetone was 0.30 GJ/kg, and for succinic acid was 0.13 GJ/kg [64].

The third analyzed parameter was the global production yield. This metric measures the production ration of generated products from the mass flow of processed feedstock, indicating how much a process took advantage of the chemical composition of the primary raw material. In the case of topology 1, this quantity corresponded to 0.17 kg of ABE products per kg of biomass. This value is within the expected production rate for this type of process [65]. Topology 2 obtained a higher production rate with a global yield of 0.43 kg of combined ethanol/succinic acid per kg of biomass. Zondervan et al. [57] synthesized a biorefinery design based on a mathematical programming approach that produced both ethanol and succinic acid with a rate of 0.26 kg per kg of biomass. Comparing that result with the outcome obtained in this study, the simulation presented in this work for topology 1 even showed a higher product yield, confirming that the models and technologies included were adequate for this kind of processing.

As expected, the total material consumption was higher for topology 2 with a total mass usage of 284,758.03 kg (or 284.76 t), while topology 1 used 120,150.04 kg (or 120.15 t). Relevant aspects are associated with a process that handles sizeable mass inventory. These can include an increase in both operating and fixed cost [66], process inherent safety [67], or in energy supply [68]. It is needed to highlight that the total amount of mass just gives an idea of the capacity of the process, but this indicator might serve to normalize other technical parameters making a comparison of scenarios possible. This indicator intrinsically included the total water consumption of both processes, which is an

important parameter considering resource conservation principles. In this sense, topology 1 showed a total water usage of 74,628.70 kg/h, equivalent to a normalized indicator of 0.62 kg of water per kg of total mass. In the case of topology 2, these parameters corresponded to 221,398.02 kg/h and 0.78 kg of water per kg of total mass. These results indicate that topology 2 demanded more water per kg of processed mass than topology 1. It could be insightful to implement mass targeting in order to seek improvement opportunities by implementing water recycling and mass integration [69]. The above might allow decreasing not just water usage but also can lead to advance side performance indicators of both processes.

3.2. Results for Environmental Assessment under the WAR Method

As described in the Methods section, this study chose the WAR algorithm to evaluate and compare environmental performance for modeled biorefineries for the production of acetone, butanol, and ethanol along with succinic acid. The WAR through the WAR GUI software allows one to evaluate three different energy sources (oil, gas, and coal), in this regard; this study chose gas as the baseline energy source since previous investigations have addressed that natural gas generates less environmental impacts compared with the other two options [70]. Besides, two scenarios were formulated to develop an environmental assessment for both topology 1 and topology 2. These cases were stated seeking improvement opportunities and scenario comparison to establish sources of environmental inefficiencies based on quantitative data. Likewise, Scenario 1 involved the quantification of the potential environmental impact counting contributions of mass streams of the system (inlet, outlet, and product streams) without including energy generation and supply effects. Scenario 2 included both mass and energy contributions.

3.2.1. Overall Output and Generation Rates

The first part of the analysis involved the estimation of the overall output and generation rates of PEI. As before mentioned, two scenarios are examined to seek sources of environmental issues, and the results (time basis) are shown in Figure 12. Topology 2 presented the highest rates of impact between the two processes, with an output rate of PEI of 1.30×10^4 PEI/h for scenario 1 and 1.39×10^4 for scenario 2. This outcome meant that the contributions of environmental effects due to energy generation just represented an increase of 6.92%, which is a deficient value compared with the impacts associated with substance flow. Otherwise, topology 1 obtained lower rates of PEI with an output rate of environmental impacts of 4.68×10^3 PEI/h for scenario 1 and 4.85×10^3 PEI/h for scenario 2. In the case of topology 1, the energy contribution just represented an increase of 3.63% with respect to the results obtained in scenario 1.

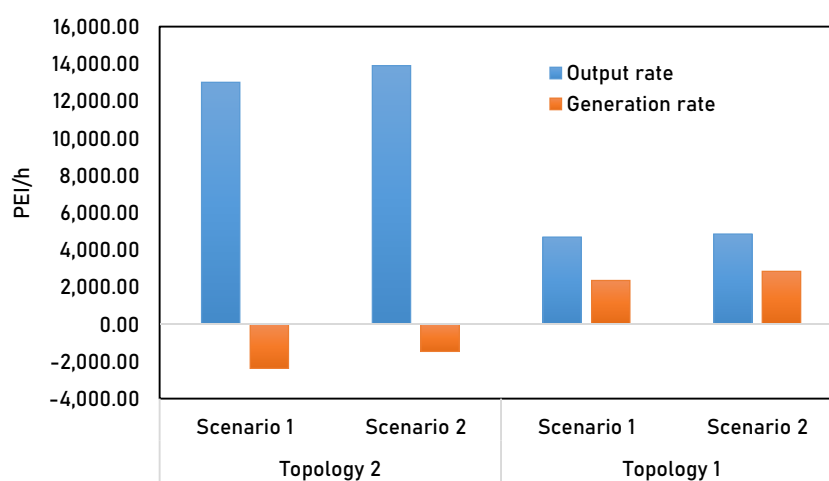


Figure 12. Overall output and generation rates (time basis) for evaluated topologies.

In terms of the generation rate of PEI, topology 2 showed negative values for both scenarios. This outcome meant that this biorefinery could transform entering raw materials into less harmful to aquatic, terrestrial, human health, and natural environment ecosystems in general. Precisely, the generation rate for scenario 1 in topology 2 corresponded to -2.73×10^3 PEI/h, while in scenario 2, this value was -1.47×10^3 PEI/h. This result might indicate that energy supply might impact the generation rate of PEI in this case, reducing its consumption rate to about 46.15%. This result is an expected value since generation or supply of energy is directly associated with the operation of the plant, and it always will tend to increase the generation rate of impacts. For topology 1, the behavior of the generation of PEI was on the contrary, showing positive rates for this category that corresponded to 2.35×10^3 PEI/h and 2.84×10^3 PEI/h for scenarios 1 and 2. Here the contribution or energy sources just implied a rise of 20.85% with respect to the base case.

Results for the overall output rates provided insightful information about the general behavior of evaluated scenarios (separately) but lacked bias considering that the size of topologies was different. The environmental analysis presented here included the estimation of both generation and output rates of PEI through a mass-product basis. This approach allows performing straightforward comparisons by normalizing environmental rates. Figure 13 displays the results for the overall output and generation rates in a mass-product basis.

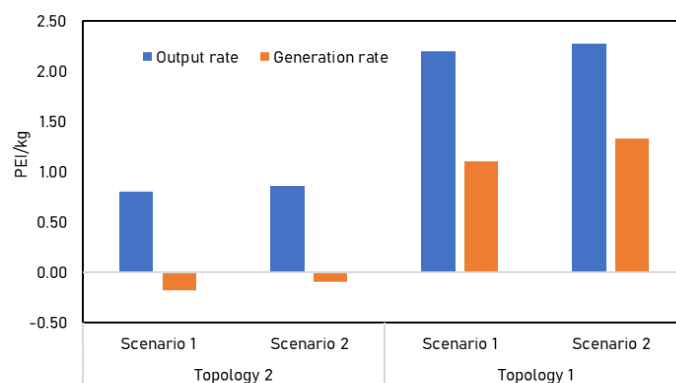


Figure 13. Overall output and generation rates (mass basis) for evaluated topologies.

According to Figure 13, topology 1 showed higher mass basis rates, with 2.20 PEI/kg for scenario 1 and 2.28 PEI/kg for scenario 2, compared with those obtained by topology 2. The last one presented 0.80 PEI/kg and 0.86 PEI/kg for scenarios 1 and 2, respectively. These outcomes evidenced that even though topology 2 obtained higher impact outlet rates, topology 1 would emit higher impacts by random discharges per kg of synthesized products. Additionally, the difference between these designs was vast, considering that topology 1 would produce 2.65 times the impacts that could be generated from topology 2. Topology 2 exhibited better environmental performance, with equivalent rates of -0.17 PEI/kg (Scenario 1) and -0.09 PEI/kg (Scenario 2), compared with those obtained by topology 1, which in both scenarios were above 1.00 PEI/kg.

3.2.2. Atmospheric Impact Categories

The analysis was also complemented with the evaluation of atmospheric impact categories for both case studies. In this sense, rates for environmental impacts on the mass basis were used to compare both bioprocesses. Figure 14 shows generation rates of PEI for atmospheric categories of both topologies.

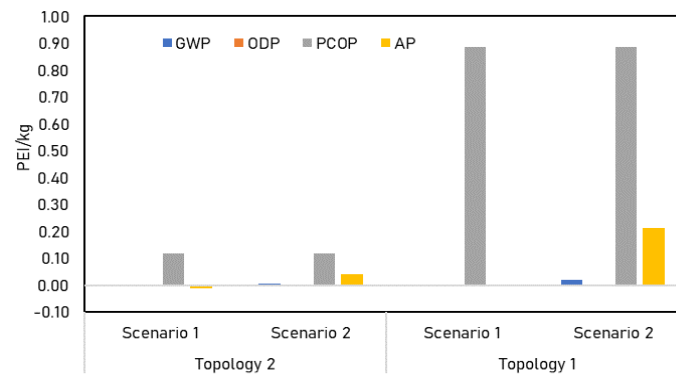


Figure 14. Generation rates of potential environmental impact (PEI) for atmospheric categories.

This section of the analysis revealed that topology 1 showed higher rates for generation of environmental impacts than topology 2, especially in PCOP and AP categories. With the production of 0.885 PEI/kg for topology 2 (in both scenarios) in the photochemical oxidation potential category, while in topology 2, these rates corresponded to 0.12 PEI/kg (also in both scenarios). These results evidenced that topology 1 would generate more volume of substances that can remain over time in the atmosphere due to their low oxidation [70]. Another impacted category in topology 1 was the AP category. This fact is associated with the rates of impacts derived from energy generation.

It is worth noting that in both topologies, energy usage affects profoundly impacted this category, since for scenario 1 in topology 1, the generation rate was -4.37×10^{-5} PEI/kg, while in the same scenario for topology 2, this value corresponded to -4.41×10^{-4} PEI/kg. The obtained rates of PEI for GWP and ODP categories remained in shallow values, indicating that these bioprocesses would not represent significant concerns in terms of global atmospheric pollution over time. The analysis of atmospheric impacts also included an evaluation of the output rate of PEI for belonging categories in this group, and these results are shown in Figure 15.

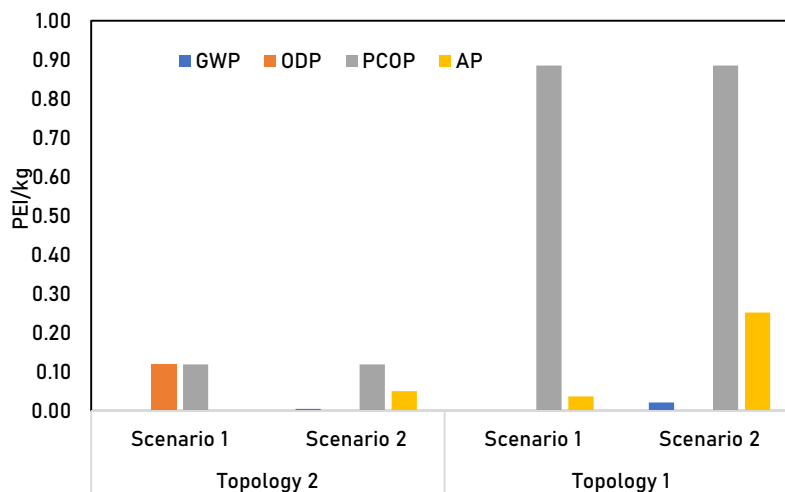


Figure 15. Output rates of PEI for atmospheric impacts.

It should be noted that the output rate of PEI refers to the possible amount of environmental impact that leaves a system together with mass and energy flows, and this quantity includes the rate of generated impacts directly derived from process operation. In this sense, it is palpable that the output rate of PEI of the PCOP category was equal to the generation rate for topology 1 (0.885 PEI/kg) and topology 2 (0.12 PEI/kg). Similar behavior was presented for the AP category. These impacts are mostly associated with product streams and energy generation that could potentially accelerate photochemical smog formation and medium acidification in these systems [71]. Comparing the obtained atmospheric

categories in both bioprocesses, it is evident that topology 2 showed better environmental performance than topology 1, with lower output rates of PEI on the mass basis in all categories.

3.2.3. Toxicological Impact Categories

As developed for atmospheric categories, this analysis included toxicological category examination through the comparison of rates of PEI in kg of product basis. Figure 16 shows the analysis of generation rates of PEI for toxicological categories.

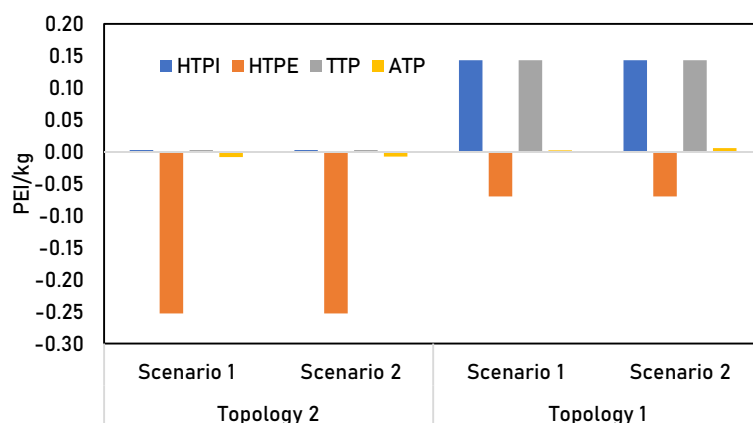


Figure 16. Generation rates of PEI for toxicological categories.

Excellent outcomes were obtained in the generation rate for the human toxicity by dermal exposure (HTPE) category in both evaluated topologies, showing negative magnitudes for this factor in all scenarios. In this sense, topology 2 obtained a rate of -0.25 PEI/kg in scenario 1 and scenario 2, while topology 1 showed -0.07 PEI/kg also in both scenarios. These results mean that the process would emit fewer toxic substances that affect human toxicity by dermal exposure or inhalation than those that entered the systems. Similar behavior was evidenced in topology 2 for human toxicity by ingestion (HTPI), terrestrial toxicity potential (TTP), and aquatic toxicity potential (ATP) categories but with lower rates of environmental impact consumption. Otherwise, topology 1 showed generation rates of PEI for HTPI and TTP categories of 0.143 PEI/kg in both scenarios, firsts indicating that this process generates associated impacts in human and terrestrial toxicity. In a second case, these results evidenced that the energy supply did not affect the generation of impacts in the toxicological categories. As developed for the previous section, the analysis presented the examination of the output rates of PEI for the toxicological group, and these results are shown in Figure 17.

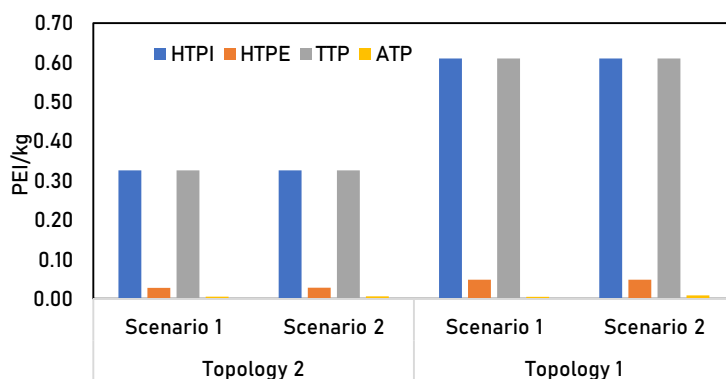


Figure 17. Output rates of PEI for toxicological categories.

According to the results of Figure 17, topology 1 presented moderately higher output rates of PEI for all toxicological categories in both scenarios. It is worth highlighting that the contribution

of energy generation in the outlet rates of PEI for this group of categories was practically neglected. The above indicated that the energy impact in environmental behavior mostly affected PCOP and AP categories, which is an expected result for this type of design [72]. In both topologies, HTPI and TTP were the most impacted categories with output rates of PEI of 0.326 PEI/kg for topology 1 and 0.610 PEI/kg for topology 2. Nevertheless, it should be mentioned that these values remained within low values for this type of processing, confirming the excellent environmental performance of both designs [73]. Furthermore, the developed analysis of toxicological categories, along with the overall and atmospheric category examination, evidenced that topology 1 might represent a better alternative for biomass transformation, as demonstrated by its higher environmental performance.

4. Conclusions

This study presented a computer-aided simulation and evaluation of topological biorefinery pathways, for in a first case, a coproduction of ABE products, and in a second case, synthesis of succinic acid and ethanol. The above was accomplishing employing process simulation through Aspen Plus[®] software and the waste reduction algorithm. Results revealed that there was a promising production of valuable products from the use of current available lignocellulosic biomasses in the North Colombia region. With a production capacity of 546.3 kg/h of acetone, 280.0 kg/h of ethanol, and 1305 kg/h of butanol in biorefinery design 1, while biorefinery design 2 could produce 13,865.7 kg/h of acetic acid and 2277.9 kg/h of ethanol. Evaluated technical data also evidenced that both topologies employed several external resources for their production processes. This outcome may represent a real drawback in the development of this type of technology as a result of high current energy and water supply–demand. In this sense, it makes sense to mention that topology 2 showed a higher performance concerning evaluated technical parameters than the results obtained by topology 1.

Regarding results provided by the environmental analysis, these indicated that from a global point of view, topology 1 presented higher rates of environmental impacts, which evidenced that this topology had a weaker performance from the ecological point of view. Additionally, it was determined that impacts associated with energy generation did not affect the environmental performance in both designs. This outcome was a positive finding since energy supply was evaluated from natural gas (fossil fuel) usage, and this source might not affect the life cycle of the system. In summary, topology 2 seemed to be the most convenient design between examined topologies under the methods and indicators implemented in this work. Directions for future works might involve the inclusion of side indicators for studying more in detail other technical aspects that can include process economics under uncertainty, principles of the circular economy, process safety, or exergetic analysis. Besides, the proposed designs can be further improved by implementing methodologies for process integration or intensification, which could permit better use of their resources. The above also might implicate consideration of burning in a broiler or anaerobic digestion to reduce energy requirements for the whole process.

Author Contributions: Conceptualization, S.I.M.-H., and P.P.; methodology, S.I.M.-H., and P.P.; software, J.R.; validation, J.R. and P.P.; resources, J.R.; programming, S.I.M.-H.; writing, S.I.M.-H.; review and editing, S.I.M.-H., P.P., and J.R.; supervision, P.P. and J.R.; project administration, J.R.; funding acquisition, J.R. All authors have read and agreed to the published version of the manuscript.

Funding: This research and the APC were funded through the strengthening and sustainability plan of the research groups of the Universidad de Cartagena.

Acknowledgments: The authors want to thank the Universidad de Cartagena for its support in the development of this research.

Conflicts of Interest: The authors declare no conflict of interest.

References

1. Meramo-Hurtado, S.I.; González-Delgado, Á.D. Biorefinery synthesis and design using sustainability parameters and hierarchical/3D multi-objective optimization. *J. Clean. Prod.* **2019**, *240*, 118134. [[CrossRef](#)]
2. Foo, D. Process Integration for Resource Conservation. Available online: https://books.google.com.co/books?id=fkX7CAAQAQBAJ&pg=PA351&lpg=PA351&dq=cost+of+water+regeneration+in+recycling+networks&source=bl&ots=bRpTLejRF3&sig=ACFu3U3U_H2YJo6emoeHZ-agV3pE5N5GZA&hl=es&sa=X&ved=2ahUKEwjF3_rW2YTqAhVDTd8KHTjwABkQ6AEwAHoECAoQAQ#v=onepa (accessed on 15 July 2020).
3. Martinazzo, A.P.; Melo, E.D.C.; Barbosa, L.C.A.; Soares, N.D.F.F.; Rocha, R.P.; Randuz, L.L.; Berbert, P.A. Quality Parameters of Cymbopogon citratus Leaves During Ambient Storage. *Appl. Eng. Agric.* **2009**, *25*, 543–547. [[CrossRef](#)]
4. Fonseca, G.; Costa, C.; Cruz, A.J.G. Economic analysis of a second-generation ethanol and electricity biorefinery using superstructural optimization. *Energy* **2020**, *204*. [[CrossRef](#)]
5. Zhang, Y.; Hu, G.; Brown, R. Life cycle assessment of the production of hydrogen and transportation fuels from corn stover via fast pyrolysis. *Environ. Res. Lett.* **2013**, *8*, 025001. [[CrossRef](#)]
6. Meramo-Hurtado, S.; Alarcón-Suesca, C.; González-Delgado, Á.D. Exergetic sensibility analysis and environmental evaluation of chitosan production from shrimp exoskeleton in Colombia. *J. Clean. Prod.* **2020**, *248*, 119285. [[CrossRef](#)]
7. Hellsmark, H.; Mossberg, J.; Söderholm, P.; Frishammar, J. Innovation system strengths and weaknesses in progressing sustainable technology: The case of Swedish biorefinery development. *J. Clean. Prod.* **2016**, *131*, 702–715. [[CrossRef](#)]
8. López-Linares, J.C.; Gómez-Cruz, I.; Ruiz, E.; Romero, I.; Castro, E. Production of Ethanol from Hemicellulosic Sugars of Exhausted Olive Pomace by Escherichia coli. *Processes* **2020**, *8*, 533. [[CrossRef](#)]
9. Vikash, P.V.; Shastri, Y. Conceptual design of a lignocellulosic biorefinery and its supply chain for ethanol production in India. *Comput. Chem. Eng.* **2019**, *121*, 696–721. [[CrossRef](#)]
10. Nhien, L.C.; Long, N.V.D.; Lee, M. Novel heat-integrated and intensified biorefinery process for cellulosic ethanol production from lignocellulosic biomass. *Energy Convers. Manag.* **2017**, *141*, 367–377. [[CrossRef](#)]
11. Dávila, I.; Gullón, B.; Labidi, J.; Gullón, P. Multiproduct biorefinery from vine shoots: Bio-ethanol and lignin production. *Renew. Energy* **2019**, *142*, 612–623. [[CrossRef](#)]
12. Meramo-Hurtado, S.I.; Puella, P.; Ribón, J.C.R. Application of Solution Strategies for Numerical Estimation of Thermodynamic Equilibrium Parameters for an Acetone–Butanol Mixture. *Appl. Sci.* **2020**, *10*, 3136. [[CrossRef](#)]
13. Mahmud, M.P.; Huda, N.; Farjana, S.H.; Lang, C. Life-cycle impact assessment of renewable electricity generation systems in the United States. *Renew. Energy* **2020**, *151*, 1028–1045. [[CrossRef](#)]
14. Alonso-Fariñas, B.; Gallego-Schmid, A.; Haro, P.; Azapagic, A. Environmental assessment of thermo-chemical processes for bio-ethylene production in comparison with bio-chemical and fossil-based ethylene. *J. Clean. Prod.* **2018**, *202*, 817–829. [[CrossRef](#)]
15. Bare, J. TRACI 2.0: The tool for the reduction and assessment of chemical and other environmental impacts 2.0. *Clean Technol. Environ. Policy* **2011**, *13*, 687–696. [[CrossRef](#)]
16. Barrett, W.M.; Van Baten, J.; Martin, T.M. Implementation of the waste reduction (WAR) algorithm utilizing flowsheet monitoring. *Comput. Chem. Eng.* **2011**, *35*, 2680–2686. [[CrossRef](#)]
17. Fortier, M.-O.P.; Roberts, G.W.; Stagg-Williams, S.M.; Sturm, B.S. Life cycle assessment of bio-jet fuel from hydrothermal liquefaction of microalgae. *Appl. Energy* **2014**, *122*, 73–82. [[CrossRef](#)]
18. Moreno-Sader, K.; Meramo-Hurtado, S.I.; González-Delgado, Á.D. Computer-aided environmental and exergy analysis as decision-making tools for selecting bio-oil feedstocks. *Renew. Sustain. Energy Rev.* **2019**, *112*, 42–57. [[CrossRef](#)]
19. Alonso-Fariñas, B.; Oliva, A.; Rodríguez-Galán, M.; Esposito, G.; Martin, J.F.G.; Rodríguez-Gutiérrez, G.; Serrano, A.; Feroso, F. Environmental Assessment of Olive Mill Solid Waste Valorization via Anaerobic Digestion Versus Olive Pomace Oil Extraction. *Processes* **2020**, *8*, 626. [[CrossRef](#)]

20. Niño-López, L.; Cárdenas, A.A.; Zambrano, R.G. Evaluation of Chemical Pretreatments for Enzymatic Hydrolysis of Lignocellulosic Residues Cassava (*Manihot Esculenta* Crantz). Available online: http://www.scielo.org.co/scielo.php?script=sci_arttext&pid=S0120-62302013000400025&lng=en&nrm=iso&tlng=es (accessed on 15 July 2020).
21. Igbínádólor, R.O.; Onilude, A.A. Bioprocess systems applied for the production of bio-ethanol from lignocellulosic biomass of cocoa pod husk (*Theobroma cacao* L.) and other agricultural residues: A review. *Afr. J. Biotechnol.* **2013**, *12*, 5375–5388. [[CrossRef](#)]
22. Meramo-Hurtado, S.I.; Sanchez-Tuiran, E.; Ponce-Ortega, J.M.; El-Halwagi, M.M.; Ojeda-Delgado, K.A. Synthesis and Sustainability Evaluation of a Lignocellulosic Multifedstock Biorefinery Considering Technical Performance Indicators. *ACS Omega* **2020**, *5*, 9259–9275. [[CrossRef](#)]
23. Li, M.; Cao, S.; Meng, X.; Studer, M.H.; Wyman, C.E.; Ragauskas, A.J.; Pu, Y. The effect of liquid hot water pretreatment on the chemical–structural alteration and the reduced recalcitrance in poplar. *Biotechnol. Biofuels* **2017**, *10*, 237. [[CrossRef](#)] [[PubMed](#)]
24. Lodi, G.U.; De Guido, G.; Pellegrini, L.A. Simulation and energy analysis of the ABE fermentation integrated with gas stripping. *Biomass-Bioenergy* **2018**, *116*, 227–235. [[CrossRef](#)]
25. Qing, Q.; Yang, B.; Wyman, C.E. Xylooligomers are strong inhibitors of cellulose hydrolysis by enzymes. *Bioresour. Technol.* **2010**, *101*, 9624–9630. [[CrossRef](#)] [[PubMed](#)]
26. Niglio, S.; Marzocchella, A.; Rehmann, L. Clostridial conversion of corn syrup to Acetone-Butanol-Ethanol (ABE) via batch and fed-batch fermentation. *Heliyon* **2019**, *5*, e01401. [[CrossRef](#)] [[PubMed](#)]
27. Kaymak, D.B. A novel process design for biobutanol purification from ABE fermentation. *Chem. Eng. Trans.* **2018**, *69*, 445–450.
28. Liu, Q.; Li, W.; Ma, Q.; An, S.; Li, M.; Jameel, H.; Chang, H.-M. Pretreatment of corn stover for sugar production using a two-stage dilute acid followed by wet-milling pretreatment process. *Bioresour. Technol.* **2016**, *211*, 435–442. [[CrossRef](#)]
29. De Jong, E.; Gosselink, R.J. Lignocellulose-Based Chemical Products. *Bioenerg. Res. Adv. Appl.* **2014**, 277–313. [[CrossRef](#)]
30. Luo, L.; Van Der Voet, E.; Huppel, G. Biorefining of lignocellulosic feedstock—Technical, economic and environmental considerations. *Bioresour. Technol.* **2010**, *101*, 5023–5032. [[CrossRef](#)]
31. Meramo-Hurtado, S.I.; Ojeda, K.A.; Sanchez-Tuiran, E. Environmental and Safety Assessments of Industrial Production of Levulinic Acid via Acid-Catalyzed Dehydration. *ACS Omega* **2019**, *4*, 22302–22312. [[CrossRef](#)]
32. Wooley, R.; Ruth, M.; Sheehan, J.; Majdeski, H.; Galvez, A. Lignocellulosic Biomass to Ethanol Process Design and Economics Utilizing Co-Current Dilute Acid Prehydrolysis and Enzymatic Hydrolysis Current and Futuristic Scenarios Lignocellulosic Biomass to Ethanol Process Design and Economics Utilizing Co-Current, D. Contract. Available online: <http://devafdc.nrel.gov/pdfs/3957.pdf> (accessed on 15 July 2020).
33. Kumar, D.; Murthy, G.S. Impact of pretreatment and downstream processing technologies on economics and energy in cellulosic ethanol production. *Biotechnol. Biofuels* **2011**, *4*, 27. [[CrossRef](#)]
34. Wooley, R.; Putsche, V. *Development of an ASPEN PLUS Physical Property Database for Biofuels Components*. (No. NREL/TP-425-20685); National Renewable Energy Lab.: Golden, CO, USA, 1996.
35. Jacquet, N.; Maniet, G.; Vanderghem, C.; Delvigne, F.; Richel, A. Application of Steam Explosion as Pretreatment on Lignocellulosic Material: A Review. *Ind. Eng. Chem. Res.* **2015**, *54*, 2593–2598. [[CrossRef](#)]
36. Millat, T.; Winzer, K. Mathematical modelling of clostridial acetone-butanol-ethanol fermentation. *Appl. Microbiol. Biotechnol.* **2017**, *101*, 2251–2271. [[CrossRef](#)] [[PubMed](#)]
37. Qureshi, N.; Saha, B.C.; Cotta, M.A.; Singh, V. An economic evaluation of biological conversion of wheat straw to butanol: A biofuel. *Energy Convers. Manag.* **2013**, *65*, 456–462. [[CrossRef](#)]
38. Lin, Z.; Liu, H.; Yan, X.; Zhou, Y.; Cheng, K.-K.; Zhang, J. High-efficiency acetone-butanol-ethanol production and recovery in non-strict anaerobic gas-stripping fed-batch fermentation. *Appl. Microbiol. Biotechnol.* **2017**, *101*, 8029–8039. [[CrossRef](#)] [[PubMed](#)]
39. Paniagua-García, A.I.; Hijosa-Valsero, M.; Díez-Antolínez, R.; Sánchez, M.E.; Coca, M. Enzymatic hydrolysis and detoxification of lignocellulosic biomass are not always necessary for ABE fermentation: The case of *Panicum virgatum*. *Biomass Bioenerg.* **2018**, *116*, 131–139. [[CrossRef](#)]
40. Martínez-Moreno, R.; Morales, P.; Gonzalez, R.; Mas, A.; Beltran, G. Biomass production and alcoholic fermentation performance of *Saccharomyces cerevisiae* as a function of nitrogen source. *FEMS Yeast Res.* **2012**, *12*, 477–485. [[CrossRef](#)]

41. Haigh, K.; Petersen, A.M.; Gottumukkala, L.; Mandegari, M.A.; Naleli, K.; Görgens, J. Simulation and comparison of processes for biobutanol production from lignocellulose via ABE fermentation. *Biofuels Bioprod. Biorefining* **2018**, *12*, 1023–1036. [CrossRef]
42. Sarchami, T.; Munch, G.; Johnson, E.; Kießlich, S.; Rehmann, L. A Review of Process-Design Challenges for Industrial Fermentation of Butanol from Crude Glycerol by Non-Biphasic *Clostridium pasteurianum*. *Fermentation* **2016**, *2*, 13. [CrossRef]
43. Friedl, A. Downstream process options for the ABE fermentation. *FEMS Microbiol. Lett.* **2016**, *363*. [CrossRef]
44. Kaymak, D.B. Design and Control of an Alternative Process for Biobutanol Purification from ABE Fermentation. *Ind. Eng. Chem. Res.* **2019**, *58*, 1957–1965. [CrossRef]
45. Lodi, G.; Pellegrini, L.A. Recovery of Butanol from ABE Fermentation Broth by Gas Stripping. *Chem. Eng. Trans.* **2016**, *49*, 13–18.
46. Da Silva, A.R.G.; Giuliano, A.; Errico, M.; Rong, B.-G.; Barletta, D. Economic value and environmental impact analysis of lignocellulosic ethanol production: Assessment of different pretreatment processes. *Clean Technol. Environ. Policy* **2019**, *21*, 637–654. [CrossRef]
47. Kang, Q.; Huybrechts, J.; Van Der Bruggen, B.; Baeyens, J.; Tan, T.; Dewil, R. Hydrophilic membranes to replace molecular sieves in dewatering the bio-ethanol/water azeotropic mixture. *Sep. Purif. Technol.* **2014**, *136*, 144–149. [CrossRef]
48. Meramo-hurtado, S.I.; Gonza, A.D.; Rehmann, L.; Quin, E.; Mehrvar, M. Comparison of Biobutanol Production Pathways via Acetone—Butanol—Ethanol Fermentation Using a Sustainability Exergy-Based Metric. *ACS Omega* **2020**, *5*, 18710–18730. [CrossRef] [PubMed]
49. Meramo-Hurtado, S.; Ojeda-Delgado, K.; Sanchez-Tuiran, E. Exergy analysis of bioethanol production from rice residues. *Contemp. Eng. Sci.* **2018**, *11*, 467–474. [CrossRef]
50. Luthfi, A.A.I.; Jahim, J.M.; Harun, S.; Tan, J.P.; Mohammad, A.W. Biorefinery approach towards greener succinic acid production from oil palm frond bagasse. *Process. Biochem.* **2016**, *51*, 1527–1537. [CrossRef]
51. Fu, N.; Peiris, P.; Markham, J.; Bavor, J. A novel co-culture process with *Zymomonas mobilis* and *Pichia stipitis* for efficient ethanol production on glucose/xylose mixtures. *Enzym. Microb. Technol.* **2009**, *45*, 210–217. [CrossRef]
52. Shanmugam, S.; Balasubramaniyan, B.; Jayaraman, J.; Ramanujam, P.K.; Gurunathan, B. Simultaneous saccharification and fermentation of bioethanol from softwood moringa oleifera using thermo-tolerant yeast *Kluyveromyces marxianus* MTCC 1388. *Int. J. ChemTech Res.* **2014**, *6*, 5118–5124.
53. Buruiană, C.-T.; Vizireanu, C.; Garrote, G.; Parajó, J. Optimization of corn stover biorefinery for coproduction of oligomers and second generation bioethanol using non-isothermal autohydrolysis. *Ind. Crop. Prod.* **2014**, *54*, 32–39. [CrossRef]
54. Afzal, S.; Sengupta, D.; Sarkar, A.; El-Halwagi, M.M.; Elbashir, N. Optimization Approach to the Reduction of CO₂ Emissions for Syngas Production Involving Dry Reforming. *ACS Sustain. Chem. Eng.* **2018**, *6*, 7532–7544. [CrossRef]
55. González-Delgado, Á.D.; Kafarov, V. Microalgae based biorefinery: Issues to consider. *CT&F—Ciencia, Tecnología y Futuro* **2011**, *4*, 5–21. [CrossRef]
56. Olajuyin, A.M.; Yang, M.; Liu, Y.; Mu, T.; Tian, J.; Adaramoye, O.A.; Xing, J. Efficient production of succinic acid from *Palmaria palmata* hydrolysate by metabolically engineered *Escherichia coli*. *Bioresour. Technol.* **2016**, *214*, 653–659. [CrossRef] [PubMed]
57. Zondervan, E.; Nawaz, M.; De Haan, A.B.; Woodley, J.M.; Gani, R. Optimal design of a multi-product biorefinery system. *Comput. Chem. Eng.* **2011**, *35*, 1752–1766. [CrossRef]
58. USEPA. Waste Reduction Algorithm: Chemical Process Simulation for Waste Reduction. Available online: <https://www.epa.gov/chemical-research/waste-reduction-algorithm-chemical-process-simulation-waste-reduction> (accessed on 15 July 2020).
59. Young, U.M.; Cabezas, H. Designing sustainable processes with simulation: The waste reduction (WAR) algorithm. *Comput. Chem. Eng.* **1999**, *23*, 1477–1491. [CrossRef]
60. Moreno-Sader, K.; Meramo-Hurtado, S.; González-Delgado, Á.D. Environmental sustainability analysis of chitosan microbeads production for pharmaceutical applications via computer-aided simulation, WAR and TRACI assessments. *Sustain. Chem. Pharm.* **2020**, *15*, 100212. [CrossRef]
61. Young, D.M.; Scharp, R.; Cabezas, H. The waste reduction (WAR) algorithm: Environmental impacts, energy consumption, and engineering economics. *Waste Manag.* **2000**, *20*, 605–615. [CrossRef]

62. Leong, C.T.; Shariff, A.M. Process route index (PRI) to assess level of explosiveness for inherent safety quantification. *J. Loss Prev. Process. Ind.* **2009**, *22*, 216–221. [[CrossRef](#)]
63. Ruiz-Mercado, G.J.; Smith, R.L.; Gonzalez, M.A. Sustainability Indicators for Chemical Processes: I. Taxonomy. *Ind. Eng. Chem. Res.* **2012**, *51*, 2309–2328. [[CrossRef](#)]
64. Muse, J.K.; Allen, A. Energy Analysis of Butanol Extraction Using Supercritical Carbon Dioxide. Worcester Polytechnic Institute. 2017. Available online: <https://digitalcommons.wpi.edu/mqp-all/3282> (accessed on 15 July 2020).
65. Darkwah, K.; Nokes, S.E.; Seay, J.; Knutson, B.L. Mechanistic simulation of batch acetone–butanol–ethanol (ABE) fermentation with in situ gas stripping using Aspen Plus™. *Bioprocess Biosyst. Eng.* **2018**, *41*, 1283–1294. [[CrossRef](#)]
66. Cogollo-Herrera, K.; Bonfante-Álvarez, H.; De Ávila-Montiel, G.; Barros, A.H.; González-Delgado, Á.D. Techno-economic sensitivity analysis of large scale chitosan production process from shrimp shell wastes. *Chem. Eng. Trans.* **2018**, *70*, 2179–2184.
67. Qi, M.; Zhu, J.; Xu, J.; Zhao, D.; Liu, Y. Investigation of Inherently Safer Design Through Process Intensification: Novel Safety Assessment Methodology and Case Study in C3–Alkyne Hydrogenation Distillation Process. *Ind. Eng. Chem. Res.* **2019**, *58*, 4866–4880. [[CrossRef](#)]
68. Čuček, L.; Dong, X.; Klemeš, J.J.; Kravanja, Z. Total footprints-based multi-criteria optimisation of regional biomass energy supply chains. *Energy* **2012**, *44*, 135–145. [[CrossRef](#)]
69. Al-Otaibi, M.; El-Halwagi, M.M. Targeting Techniques for Enhancing Process Yield. *Chem. Eng. Res. Des.* **2006**, *84*, 943–951. [[CrossRef](#)]
70. Meramo-Hurtado, S.I.; Urbina-Suaréz, N.; González-Delgado, Á.D. Computer-aided environmental and exergy analyses of a large-scale production of chitosan microbeads modified with TiO₂ nanoparticles. *J. Clean. Prod.* **2019**, *237*. [[CrossRef](#)]
71. Abas, M.R.B.; Mohamad, S. Hazardous (organic) air pollutants. In *Encyclopedia of Environmental Health*; Elsevier: Amsterdam, The Netherlands, 2019; pp. 405–416.
72. Meramo, S. Evaluacion ambiental de una biorrefineria para produccion de maiz. *Ahead-Adelante* **2016**, *7*, 40–46.
73. Moreno-Sader, K.; Alarcón-Suesca, C.; González-Delgado, Á.D. Application of environmental and hazard assessment methodologies towards the sustainable production of crude palm oil in North-Colombia. *Sustain. Chem. Pharm.* **2020**, *15*, 100221. [[CrossRef](#)]



© 2020 by the authors. Licensee MDPI, Basel, Switzerland. This article is an open access article distributed under the terms and conditions of the Creative Commons Attribution (CC BY) license (<http://creativecommons.org/licenses/by/4.0/>).